Pergamon

Cement and Concrete Research 32 (2002) 1347–1356

CEMENT AND CONCRETE RESEARCH

The superstructure of C_3S from synchrotron and neutron powder diffraction and its role in quantitative phase analyses

Ángeles G. De La Torre[a], Sebastián Bruque[a], Javier Campo[b,c], Miguel A.G. Aranda[a,*]

[a]*Departamento de Química Inorgánica, Universidad de Málaga, 29071 Málaga, Spain*
[b]*Institut Laue-Langevin, B.P. 156, 38042 Grenoble Cedex 9, France*
[c]*Instituto de Ciencia de Materiales de Aragón, CSIC-Universidad de Zaragoza, 50009 Zaragoza, Spain*

Received 29 June 2001; accepted 26 February 2002

Abstract

We have synthesised the room temperature MIII form of alite stabilised by doping with Mg and Al. The complex disordered superstructure of this tricalcium silicate [Ca_3SiO_5 (C_3S)] sample has been studied by a joint Rietveld refinement of ultra-high-resolution synchrotron X-ray powder diffraction data, medium-resolution neutron powder diffraction data and soft constraints of interatomic distances. Alite crystallises in a monoclinic cell with dimensions $a = 33.1078(6)$ Å, $b = 7.0355(1)$ Å, $c = 18.5211(4)$ Å, $\beta = 94.137(1)°$ and $V = 4302.9(2)$ Å^3. The final R factors were $R_{WP} = 8.76\%$ and $R_F(C_3S) = 3.45\%$ for the synchrotron data and $R_{WP} = 6.09\%$ and $R_F(C_3S) = 5.10\%$ for the neutron data. The reported superstructure is simpler than those previously reported, and it fits properly to a variety of Portland clinker and cement patterns. The Rietveld analyses of four clinkers with variable Mg contents have shown that the refinements are good. The Bogue approach gave quite poor results when compared to these state-of-the-art powder diffraction analyses. Bogue method slightly underestimates the $C_3S + C_2S$ content, overestimates the C_3A fraction and underestimates the C_4AF content. Similar analyses of Portland cements with nine crystalline phases are shown to be feasible.

Keywords: X-ray diffraction; Characterization; Rietveld method; Ca_3SiO_5

1. Introduction

There is a great deal of interest in determining the mineralogical composition of cements from laboratory X-ray powder diffraction (LXRPD) data. These analyses will allow to routinely assess the quality of the cements off-line. The methodology can also be used to monitor the production process on-line. A prototype of such system has been recently developed, and it allows to follow the mineralogical compositions of the clinker and cement streams on-line in a factory [1,2]. To date, there are several recent examples of quantitative phase studies, including Portland cements [3–9], aluminous cements [10] and calcium sulpho-aluminate cements [11], by powder diffraction. Sometime ago, several approaches were used to analyse the powder diffraction pattern of Portland cements [12–15], but nowadays, the reports [1–11] use the Rietveld method [16–18] to quantify the crystalline components. The quantitative phase analysis using the Rietveld method consists of the comparison between the measured and the calculated patterns, so, it does not need internal standard, but the crystal structures of all components must be known.

On the other hand, tricalcium silicate [Ca_3SiO_5 (C_3S)] is probably the most important component of Portland cements. The crystal structure of the stable room temperature (RT) polymorph of stoichiometric C_3S is triclinic and known [19,20]. Stoichiometric C_3S exhibits seven polymorphs [21]: three triclinics (TI, TII, TIII), three monoclinics (MI, MII, MIII) and one rhombohedral (R). The phase transformations are TI⇆TII⇆TIII⇆MI⇆MII⇆MIII⇆R at 620, 920, 980, 990,1060 and 1070 °C, respectively. However, the presence of foreign ions may stabilise some of the high-temperature polymorphs at RT. For instance, Mg^{2+} cations stabilise the MIII monoclinic form. This ‘‘polymorph’’, alite, is very important because it is the main component of Portland clinker and cements [3,21,22]. The crystal structure of

* Corresponding author. Tel.: +34-9-5213-1874; fax: +34-9-5213-2000.
E-mail address: g_aranda@uma.es (M.A.G. Aranda).

0008-8846/02/$ – see front matter
PII: S0008-8846(02)00796-2

monoclinic MIII C_3S is not simple. Mg-doped C_3S crystallises at RT in a monoclinic subcell with the following parameters: $a = 12.2$ Å, $b = 7.0$ Å, $c = 9.3$ Å and $\beta = 116.3°$ [23]. The true cell is sometimes much larger with the following dimensions: $a = 33.1$ Å, $b = 7.0$ Å, $c = 18.5$ Å and $\beta = 94.1°$; ($3 \times 1 \times 2$ superstructure). A crystallographic description for this RT monoclinic superstructure from a tiny doped single crystal was reported [24]. Structural studies of different polymorphs, TI [19], MIII [24] and R [25], have clarified that the orientation of silicate tetrahedra plays a key role for determining the symmetry of these compounds. It is also known that this orientation at RT is induced by the presence of foreign cations such as Mg. However, the disorder, and even the presence of the superstructure itself in alite is composition and thermal history dependent as previously pointed out [23].

The final objective of our project is to demonstrate that precise and accurate analyses of Portland clinker and cements are feasible. To do so, we need a good structural description of the main phase, alite, which is also present in other industrially important compound such as slags or some high temperature refractories. Hence, we report a joint X-ray synchrotron and neutron powder diffraction (NPD) Rietveld study of alite. Our structural description fits the Portland patterns slightly better than the previously reported superstructure [24] and much better than the reported substructure [23]. This is illustrated by the analyses of alite, four clinkers and four cements. The quantitative phase studies using powder diffraction will be compared to those obtained by the Bogue calculations.

2. Experimental section

Stabilised-by-doping RT monoclinic C_3S was prepared as previously reported [26]. A mixture of the appropriated amounts of $CaCO_3$ (99.5% from Prolabo), $Mg(OH)_2{\cdot}4Mg\text{-}4MgCO_3{\cdot}5H_2O$ (99% from Aldrich), SiO_2 (99.7% from ABCR) and γ-Al_2O_3 (99.997% from Alfa) was prepared to obtain 5 g of $(Ca_{2.93}Mg_{0.07})O_3(SiO_2)_{0.98}(Al_2O_3)_{0.01}$. The sources for Mg and Al were chosen because of their high reactivities. The mixture was ground in an agate ball mill at 200 rpm for 30 min and then heated at 1050 °C in a Pt crucible for 4 h. The resulting solid was ground in an agate ball mill at 200 rpm for 30 min, pelletised, heated in air at 1450 °C for 6 h and cooled. Finally, the mixture was ground again in an agate mortar, pelletised, heated in air at 1500 °C for 6 h and cooled.

A synchrotron X-ray powder diffraction (SXRPD) pattern for C_3S was collected on the BM16 diffractometer of ESRF (Grenoble, France) in the standard Debye–Scherrer configuration. The sample was loaded in a borosilicate glass capillary ($\phi = 2.0$ mm) and rotated during data collection. A short penetrating wavelength, $\lambda = 0.450294(6)$ Å (27.54 keV), was selected with a double-crystal Si (111) monochromator and was calibrated with Si NIST ($a = 5.43094$ Å). The overall measuring time was 3 h to have good statistics over the angular range 4–30° (in 2θ) [6.45–0.87 Å]. The raw data were summed up to 0.005° step size with local software. A NPD pattern for the same sample was collected at ILL (Grenoble, France) on the high-resolution diffractometer, D1A, with $\lambda = 1.911$ Å, counting for 12 h. The 2θ range was 10–150° [10.96–0.99 Å] and the step size was 0.05°. The standard configuration, with the sample in a vanadium can with diameter of 6 mm, was used.

In order to test the structure that came out of the joint SXRPD and NPD Rietveld refinement, we have analysed four Portland clinkers and four Portland cements. Hereafter, the clinkers are labelled A1, A2, A3 and A4, and the cements are labelled B1, B2, B3 and B4. The elemental compositions were determined by X-ray fluorescence (XRF) on a Philips PW 1660 spectrometer using the borate glass bead sample preparation method, which minimises matrix effects. The clinkers and cements were sampled from the Goliat factory (Málaga, Spain).

We had collected SXRPD data for A2 clinker as previously reported [3]. We have collected LXRPD data for the remaining seven samples on a Siemens D5000 θ/2θ diffractometer (flat reflection mode). The wavelength, $CuK_{\alpha 1,2}$ 1.542 Å ($\equiv 8.04$ keV), was selected with a secondary curved graphite monochromator. The finely ground samples were placed in a methacrylate holder by side loading [27] in order to minimise preferred orientation. The 2θ range was 10–70°, in 0.03° steps, counting by 25 s per step. The holder was not spun during data collection.

3. Results and discussion

3.1. Structural study of alite

As an initial characterization, the LXRPD pattern for C_3S was indexed in the reported superstructure with unit cell dimension of $33 \times 7 \times 18$ Å ($Z = 36$). The ^{29}Si MAS NMR spectrum for C_3S agrees very well with that previously reported for the MIII polymorph [28]. Our alite presents three broad bands at $\delta = -70.31$, -73.69 and -75.84 ppm, the position of the bands previously reported were $\delta = -70.3$, -73.7 and -75.8 ppm.

It is worth pointing out that the experimental configuration used in the synchrotron X-ray structural study minimise the errors usually present in a LXRPD work. The very high energy of the synchrotron beam allows to collect the data in transmission testing a very large amount of sample without worries about absorption [$\mu(C_3S) = 8.8\ cm^{-1}$ at $\lambda = 0.45$ Å]. The rotation of the capillary avoids preferred orientation. Finally, the high energy of the X-rays also rules out extinction in the high intense peaks. NPD is usually free of such errors, and it is a complementary structural technique since it allows to accurately locate the light atoms (oxygens). Furthermore, the structure resulting from this structural study must be more representative of alite than

that determined from a tiny doped single crystal. In principle, these approaches should give the same structural result for a stoichiometric compound, but it is very important to test a large amount of sample when characterising a disordered solid solution.

We have used the superstructures of Nishi et al. [24], Berliner et al. [29–31] and Simon [30] as starting models for the joint SXRPD and NPD Rietveld refinement. The structural description given by Berliner et al. [29] led to a poorer fit, and it was not further studied. Without disorder, the monoclinic crystal structure of alite is already very complex. There are 126 crystallographically independent sites: 36 Ca [18 in special position (*x*0*z*) and 18 in general position]; 18 Si all in special position (*x*0*y*); and 72 O [54 in special position (*x*0*z*) and 18 in general position]; in the asymmetric part of the unit cell. So, this superstructure has 288 variable positional parameters plus the appropriated thermal parameters. On top of that, there is disorder in the superstructure and depending upon the used model for the disorder, the number of the structural parameters may increase dramatically.

Due to the above-discussed structural complexity, we have used a joint refinement of ultra-high-resolution synchrotron X-ray and neutron patterns to increase the number of observations (partially resolved diffraction peaks). Even in this case, the observations/refined parameters ratio was low and the joint SXRPD and NPD refinement gave some chemically unrealistic interatomic distances. Therefore, a third histogram containing soft constraints was included to have a chemically correct structural model. We have soft-constrained [17] all SiO_4 tetrahedra by imposing 96 Si–O bond distances of 1.63(3) Å and 132 O···O intratetrahedral interacting distances of 2.66(6) Å. This second set of soft constraints helps to maintain regular tetrahedral angles. We have also introduced 265 Ca–O soft constraints of 2.40(5) Å for all Ca–O distances that converged to values shorter than 2.30 Å. Similarly, we introduced 23 O···O soft constraints of 2.80(6) Å for all nonintratetrahedral O···O distances that became shorter than 2.60 Å. There is a weighting factor that allows to use this soft constraints histogram in the Rietveld procedure. High values of this parameter give more weight to the prescribed distances. As the refinement progresses, this number can be lowered allowing a better fit to the observed powder patterns but keeping a reasonable crystallochemical model. The final weighting factor for the soft constraint histogram was only −110.

Now we will focus on the disorder showed by this superstructure. The superstructure model reported by Nishi et al. [24] did not fit our powder diffraction data satisfactorily. However, a simplified model in this supercell, but without disorder, showed a much worse fit. So, to model the disorder is fundamental if we want to simulate the powder pattern properly. We have tested, as Nishi et al. did [24], the disorder of the calcium atoms. We have found that disordering the calciums located at general positions, the fit improved notably. We tested the refinement of the occupation factors of these calciums, and they converged to values close to 0.5. So, they were fixed to 1/2 and not refined. However, we have found that the disorder of the calciums at the special positions does not improve the fit significantly. The splitting of the oxide anions associated to the calcium did not also improve the fit in the joint refinement. So, in our final model, these atoms (Ca at special position and the oxygens only bonded to the calciums) are not disordered. This is a first difference with the model reported by Nishi et al. [24].

We have also checked the orientation of the silicates tetrahedra. The monoclinic substructure, $12.2 \times 7.0 \times 9.3$ $Å^3$, contains three silicate tetrahedra (triplet) arranged along the pseudo-threefold axis of the high-temperature rhombohedral structure. When the six-times-larger superstructure is taken into account, the number of tetrahedra is 18, arranged in six triplets. The relation between different C_3S polymorphs lays in the relative orientations of these tetrahedra. However, due to steric reasons, the SiO_4 tetrahedra cannot adopt all possible configurations. The direction of the pseudo-threefold axis of the true monoclinic MIII cell is along [−207] that it corresponds to the [001] axis of the R rhombohedral form. The up orientation along this axis is labelled U, the down orientation D and an intermediate disordered configuration is labelled G. We have maintained the same labelling scheme than previously reported [24,29–31] for the sake of comparison.

We have tested the relative orientation of the tetrahedra starting from the Nishi et al. [24] model and keeping the steric consideration into account. We finally concluded that eight tetrahedra are U [Si(2), Si(4), Si(5), Si(6), Si(11), Si(12), Si(15) and Si(18)] and five have the opposite configuration, D [Si(1), Si(3), Si(7), Si(13) and Si(16)]. These 13 tetrahedra are not disordered. However, three SiO_4 are disordered with fractional U and D orientations [Si(9), Si(10) and Si(14)]. Finally, the remaining two tetrahedra are out of the pseudo-threefold axis G and therefore disordered [Si(8), Si(17)]. Hence, the best agreement was obtained with the following configurations of tetrahedra: Si(1)D–Si(8)G–Si(2)U; Si(7)D–Si(9)UD–Si(10)UD; Si(3)D–Si(13)D–Si(14)UD; Si(16)D–Si(17)G–Si(5)U; Si(15)U–Si(18)U–Si(6)U and Si(11)U–Si(12)U–Si(4)U. This is the second difference with the Nishi et al. [24] model.

The ultra-high-resolution synchrotron X-ray data showed that the sample was not phase pure. The presence of dicalcium silicate (C_2S) was readily determined. Its pattern was taken into account by using the structure of Mumme et al. [36] without refining the atomic parameters. The joint refinement showed that the sample contained 5.9(2) wt.% of C_2S.

The SXRPD and NPD patterns were analysed by the Rietveld method with the GSAS suite of programs [32]. The peak shape function was pseudo-Voigt [33] for SXRPD data and Gaussian for NPD data, both corrected for axial divergence [34,35]. The backgrounds were fitted by linear interpolation function. Scale factors, cell parameters and

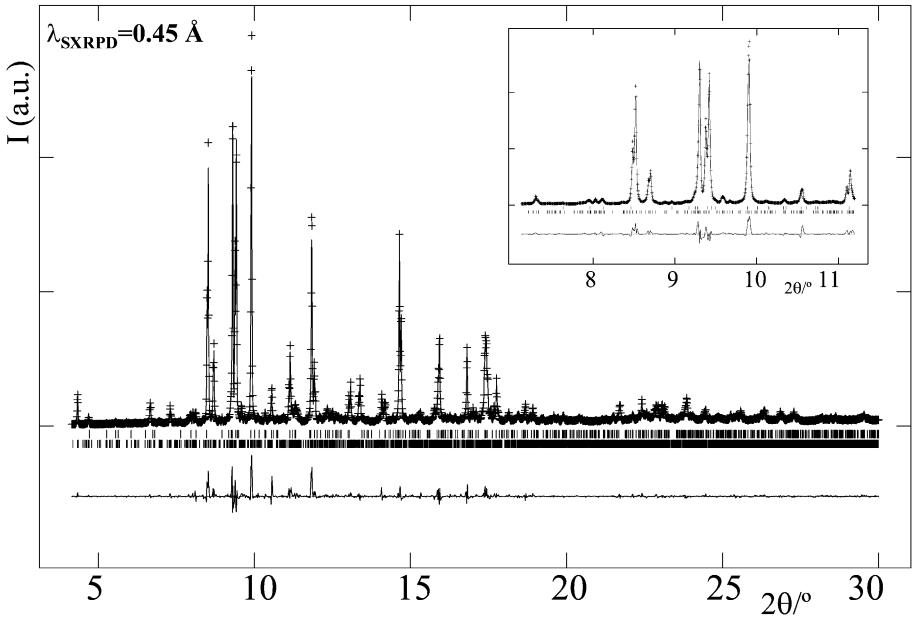

Fig. 1. SXRPD Rietveld plot for C_3S. The inset shows the fit to the most representative region for C_3S.

zero shift errors were optimised. Preferred orientation was checked, and it was found to be negligible as expected. For C_3S, the appropriated atomic parameters were refined.

The pseudo-Voigt parameters were GW (Gaussian part), LY (d^*-dependent Lorentzian part) and STEC (an ellipsoidal anisotropic correction for the Lorentzian width) along a given direction. The final values for C_3S were GW = $0.1 \times 0.01^{\circ 2}$, LY = $19.6(3) \times 0.01^{\circ}$, STE$c$ = $-2.1(5) \times 0.01^{\circ}$ along [1 0 0]. The asymmetry due to axial divergence was described with S/L = 0.0075 and H/L = 0.0058. The final Gaussian parameters to model the NPD pattern were GU = 299(38), GV = − 497(75) and GW = $483(31) \times 0.01^{\circ 2}$. The axial divergence was taken into account with S/L = 0.044 and H/L = 0.039.

A total of 472 parameters were refined in the final cycle. C_3S has $C\ m$ space group with $a = 33.1078(6)$ Å, $b = 7.0355(1)$ Å, $c = 18.5211(4)$ Å, $\beta = 94.137(1)^{\circ}$ and $V = 4302.9(2)$ Å^3. C_2S has $P\ 2_1/n$ space group with $a = 5.5087(6)$ Å, $b = 6.7594(6)$ Å, $c = 9.309(1)$ Å, $\beta = 94.464(9)^{\circ}$ and $V = 345.59(5)$ Å^3. The R factors were

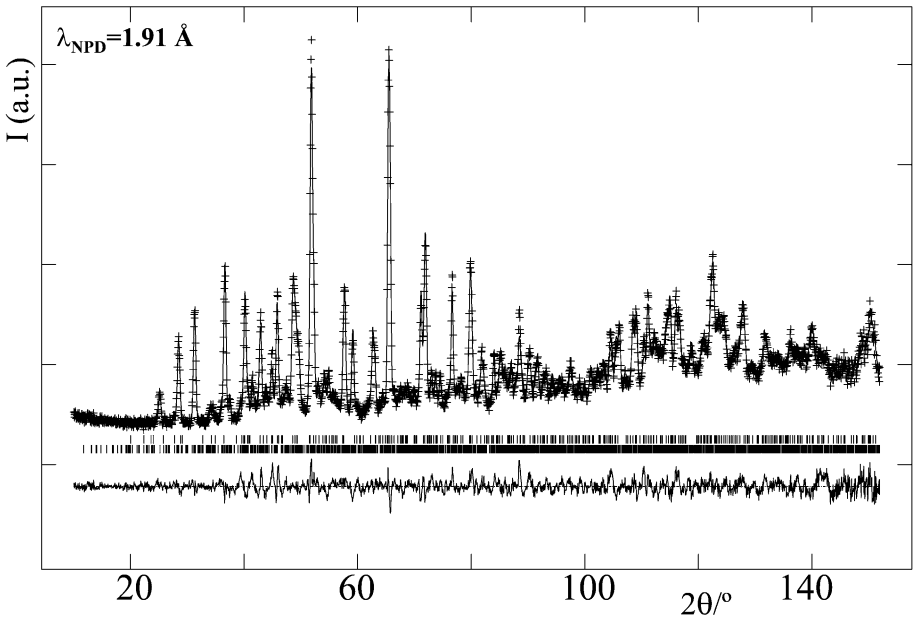

Fig. 2. NPD Rietveld plot for C_3S.

Table 1
Refined atom parameters and occupancy factors for C_3S from a joint refinement with SXRPD, NPD and soft constraints data

Atom	x	y	z	Occupation factor
Ca(1)	−0.0024(11)	0.0	0.0104(19)	1.0
Ca(2)	0.6595(10)	0.0	0.1605(19)	1.0
Ca(3)	0.3113(9)	0.0	0.3342(19)	1.0
Ca(4)	−0.0199(12)	0.0	0.4939(19)	1.0
Ca(5)	0.6531(11)	0.0	0.6651(18)	1.0
Ca(6)	0.3188(11)	0.0	0.8407(19)	1.0
Ca(7)	0.5881(11)	0.0	−0.0745(20)	1.0
Ca(8)	0.2592(11)	0.0	0.1012(19)	1.0
Ca(9)	−0.0815(11)	0.0	0.2619(19)	1.0
Ca(10)	0.5848(9)	0.0	0.4262(18)	1.0
Ca(11)	0.2494(11)	0.0	0.6061(19)	1.0
Ca(12)	−0.0817(11)	0.0	0.7649(20)	1.0
Ca(13)	0.7322(11)	0.0	−0.0925(19)	1.0
Ca(14)	0.4019(11)	0.0	0.0778(20)	1.0
Ca(15)	0.0646(10)	0.0	0.2418(19)	1.0
Ca(16)	0.7236(10)	0.0	0.4022(20)	1.0
Ca(17)	0.3895(11)	0.0	0.5731(20)	1.0
Ca(18)	0.0617(11)	0.0	0.7363(19)	1.0
Ca(19a)	−0.0835(10)	0.2749(32)	−0.0847(20)	0.5
Ca(19b)	−0.0833(10)	0.2745(31)	−0.0846(20)	0.5
Ca(20a)	0.5804(12)	0.2773(31)	0.0841(22)	0.5
Ca(20b)	0.5849(11)	0.2807(21)	0.0917(18)	0.5
Ca(21a)	0.2398(11)	0.2499(30)	0.2580(18)	0.5
Ca(21b)	0.2413(11)	0.2565(26)	0.2577(18)	0.5
Ca(22a)	−0.0969(11)	0.265(4)	0.4132(18)	0.5
Ca(22b)	−0.0938(11)	0.2926(31)	0.4099(18)	0.5
Ca(23a)	0.5759(13)	0.250(4)	0.5965(21)	0.5
Ca(23b)	0.5651(11)	0.223(4)	0.5716(24)	0.5
Ca(24a)	0.2436(11)	0.250(4)	0.7523(28)	0.5
Ca(24b)	0.2444(10)	0.2406(32)	0.7620(23)	0.5
Ca(25a)	−0.0023(14)	0.218(5)	−0.1530(25)	0.5
Ca(25b)	−0.0004(14)	0.232(5)	−0.1576(25)	0.5
Ca(26a)	0.6675(10)	0.2316(33)	0.0152(26)	0.5
Ca(26b)	0.6662(10)	0.2410(30)	0.0195(27)	0.5
Ca(27a)	0.3345(12)	0.235(4)	0.1718(21)	0.5
Ca(27b)	0.3388(10)	0.2216(27)	0.1825(18)	0.5
Ca(28a)	−0.0049(10)	0.2346(33)	0.3463(20)	0.5
Ca(28b)	−0.0051(11)	0.2382(31)	0.3444(19)	0.5
Ca(29a)	0.6608(10)	0.2289(28)	0.5199(18)	0.5
Ca(29b)	0.6570(10)	0.2178(21)	0.5225(17)	0.5
Ca(30a)	0.3312(10)	0.240(4)	0.6806(24)	0.5
Ca(30b)	0.3310(10)	0.236(4)	0.6771(28)	0.5
Ca(31a)	0.8260(13)	0.270(4)	−0.0115(21)	0.5
Ca(31b)	0.8268(10)	0.2640(30)	−0.0093(19)	0.5
Ca(32a)	0.4904(10)	0.260(4)	0.1593(19)	0.5
Ca(32b)	0.4906(10)	0.257(4)	0.1601(22)	0.5
Ca(33a)	0.1502(10)	0.254(4)	0.3293(19)	0.5
Ca(33b)	0.1509(9)	0.2540(30)	0.3288(19)	0.5
Ca(34a)	0.8127(11)	0.2600(33)	0.4928(22)	0.5
Ca(34b)	0.8139(10)	0.2611(27)	0.4998(20)	0.5
Ca(35a)	0.4826(13)	0.277(5)	0.6571(19)	0.5
Ca(35b)	0.4821(12)	0.266(4)	0.6563(19)	0.5
Ca(36a)	0.1558(11)	0.2721(31)	0.8212(19)	0.5
Ca(36b)	0.1554(10)	0.2713(27)	0.8206(18)	0.5
Si(1)	0.0816(11)	0.0	0.4254(19)	1.0
Si(2)	0.2329(11)	0.0	−0.0728(19)	1.0
Si(3)	0.4211(11)	0.0	0.7473(20)	1.0
Si(4)	0.5603(11)	0.0	0.7582(20)	1.0
Si(5)	−0.0976(10)	0.0	0.0775(17)	1.0
Si(6)	−0.1054(10)	0.0	0.5743(18)	1.0
Si(7)	0.0917(10)	0.0	−0.0895(19)	1.0
Si(8)	0.1615(10)	0.0	0.1677(18)	1.0
Si(9)	0.1588(11)	0.0	0.6621(18)	1.0
Si(10)	0.2243(9)	0.0	0.4237(17)	1.0
Si(11)	0.4176(4)	0.0	0.2554(8)	1.0
Si(12)	0.5020(10)	0.0	0.0003(19)	1.0
Si(13)	0.4845(10)	0.0	0.4913(18)	1.0
Si(14)	0.5669(9)	0.0	0.2431(17)	1.0
Si(15)	0.7532(10)	0.0	0.0911(19)	1.0
Si(16)	0.7506(10)	0.0	0.5842(19)	1.0
Si(17)	−0.1750(11)	0.0	0.3337(19)	1.0
Si(18)	−0.1757(11)	0.0	−0.1576(19)	1.0
O(1)	0.9921(13)	0.0	0.2524(21)	1.0
O(2)	0.0342(11)	0.0	0.1221(20)	1.0
O(3)	0.0309(15)	0.0	0.602(4)	1.0
O(4)	−0.0101(14)	0.0	0.7493(21)	1.0
O(5)	0.3664(11)	0.0	−0.0667(26)	1.0
O(6)	0.3313(13)	0.0	0.0836(19)	1.0
O(7)	0.2830(12)	0.0	0.2215(19)	1.0
O(8)	0.3525(13)	0.0	0.4435(22)	1.0
O(9)	0.3245(22)	0.0	0.5929(26)	1.0
O(10)	0.2857(13)	0.0	0.7233(20)	1.0
O(11)	0.6617(13)	0.0	−0.0842(21)	1.0
O(12)	0.6170(9)	0.0	0.0406(19)	1.0
O(13)	0.6976(10)	0.0	0.2982(21)	1.0
O(14)	0.6537(10)	0.0	0.4255(19)	1.0
O(15)	0.6147(11)	0.0	0.5497(20)	1.0
O(16)	0.7014(13)	0.0	0.7697(23)	1.0
O(17)	0.9399(13)	0.0	0.3866(21)	1.0
O(18)	0.9564(13)	0.0	0.9030(26)	1.0
O(D11)	0.1052(13)	0.0	0.3522(19)	1.0
O(D12)	0.0327(11)	0.0	0.4098(24)	1.0
O(D13)	0.0937(11)	0.1865(20)	0.4744(19)	1.0
O(U21)	0.2096(12)	0.0	0.0014(20)	1.0
O(U22)	0.2806(11)	0.0	−0.0530(22)	1.0
O(U23)	0.2187(11)	0.1794(17)	−0.1237(19)	1.0
O(D31)	0.4415(13)	0.0	0.6706(21)	1.0
O(D32)	0.3718(10)	0.0	0.7387(25)	1.0
O(D33)	0.4338(10)	0.1903(20)	0.7927(21)	1.0
O(U41)	0.5376(13)	0.0	0.8319(21)	1.0
O(U42)	0.6091(11)	0.0	0.7699(27)	1.0
O(U43)	0.5460(10)	0.1822(17)	0.7089(20)	1.0
O(U51)	−0.1243(12)	0.0	0.1492(19)	1.0
O(U52)	−0.0504(11)	0.0	0.1068(25)	1.0
O(U53)	−0.1067(11)	0.1899(20)	0.0297(17)	1.0
O(U61)	−0.1283(14)	0.0	0.6495(21)	1.0
O(U62)	−0.0569(10)	0.0	0.5918(24)	1.0
O(U63)	−0.1168(10)	0.1887(17)	0.5270(17)	1.0
O(D71)	0.1130(12)	0.0	−0.1667(19)	1.0
O(D72)	0.0435(10)	0.0	−0.1025(25)	1.0
O(D73)	0.1071(11)	0.1873(16)	−0.0459(19)	1.0
O(G81)	0.1382(12)	0.030(5)	0.0880(20)	0.5
O(G82)	0.1298(11)	−0.125(4)	0.2129(22)	0.5
O(G83)	0.2003(10)	−0.136(4)	0.1537(20)	0.5
O(G84)	0.1732(12)	0.1913(20)	0.2111(18)	0.5
O(D91)	0.1803(13)	0.0	0.5844(19)	0.41(3)
O(D92)	0.1104(11)	0.0	0.6479(27)	0.41(3)
O(D93)	0.1762(12)	0.1852(21)	0.7047(19)	0.41(3)
O(U94)	0.1953(13)	0.0	0.7258(25)	0.59(3)
O(U95)	0.1776(12)	0.0	0.5831(20)	0.59(3)
O(U96)	0.1303(12)	0.1876(21)	0.6686(25)	0.59(3)
O(D101)	0.2397(11)	0.0	0.3421(18)	0.41(3)
O(D102)	0.2642(13)	0.0	0.4814(21)	0.41(3)

(continued on next page)

Table 1 (*continued*)

Atom	*x*	*y*	*z*	Occupation factor
O(D103)	0.1998(11)	0.1918(16)	0.4298(21)	0.41(3)
O(U104)	0.1873(14)	0.0	0.4797(27)	0.59(3)
O(U105)	0.2644(12)	0.0	0.4777(27)	0.59(3)
O(U106)	0.2186(10)	0.1926(19)	0.3763(18)	0.59(3)
O(U111)	0.4467(10)	0.0	0.3284(15)	1.0
O(U112)	0.3699(7)	0.0	0.2682(20)	1.0
O(U113)	0.4281(9)	0.1787(21)	0.2041(15)	1.0
O(U121)	0.4706(11)	0.0	−0.0695(22)	1.0
O(U122)	0.4794(15)	0.0	0.0762(22)	1.0
O(U123)	0.5329(9)	0.1844(17)	0.0031(20)	1.0
O(D131)	0.5126(10)	0.0	0.4235(18)	1.0
O(D132)	0.4357(10)	0.0	0.4713(20)	1.0
O(D133)	0.4939(11)	0.1927(19)	0.5364(17)	1.0
O(D141)	0.5623(14)	0.0	0.1528(18)	0.41(5)
O(D142)	0.6162(10)	0.0	0.2602(24)	0.41(5)
O(D143)	0.5482(12)	0.1931(20)	0.2718(23)	0.41(5)
O(U144)	0.6030(10)	0.0	0.3053(19)	0.59(5)
O(U145)	0.5860(12)	0.0	0.1658(18)	0.59(5)
O(U146)	0.5393(9)	0.1866(17)	0.2549(19)	0.59(5)
O(U151)	0.7352(11)	0.0	0.1707(19)	1.0
O(U152)	0.7138(10)	0.0	0.0320(20)	1.0
O(U153)	0.7815(10)	0.1871(20)	0.0832(19)	1.0
O(D161)	0.7689(11)	0.0	0.5065(20)	1.0
O(D162)	0.7020(10)	0.0	0.5788(21)	1.0
O(D163)	0.7646(10)	0.1836(17)	0.6330(19)	1.0
O(G171)	−0.1969(11)	0.092(5)	0.2620(21)	0.5
O(G172)	−0.2066(13)	−0.156(5)	0.3627(29)	0.5
O(G173)	−0.1365(12)	−0.133(4)	0.3145(21)	0.5
O(G174)	−0.1556(12)	0.123(4)	0.3998(22)	0.5
O(U181)	−0.1962(11)	0.0	−0.0796(19)	1.0
O(U182)	−0.1274(11)	0.0	−0.1410(24)	1.0
O(U183)	−0.1905(12)	0.1912(20)	−0.2011(19)	1.0

The thermal factors are given in the text.

$R_{WP}=8.76\%$, $R_P=7.13\%$, $R_F(C_3S)=3.45\%$ and $R_F(C_2S)=3.23\%$ for the SXRPD data and $R_{WP}=6.09\%$, $R_P=4.95\%$, $R_F(C_3S)=5.10\%$ and $R_F(C_2S)=5.65\%$ for the NPD data. The Rietveld plot for the SXRPD data is given in Fig. 1. The inset shows the most representative Bragg peaks for C_3S. The Rietveld plot for the NPD data is given in Fig. 2.

Our structural model for the superstructure (Table 1) contains 155 sites (18 Si, 54 Ca and 83 O) with 373 refined positional parameters. Some sites are disordered with fixed, 0.5, or refined occupation factors (see Table 1). In the final model, we refined five different U_{iso} parameters: one for the Ca atoms in special position, 0.012(1) Å^2; a second for the calciums at general position, 0.0104(8) Å^2; another for the silicons, 0.004(1) Å^2; a fourth for the oxygens belonging to the SiO_4 tetrahedra, 0.016(1) Å^2; and a final one for the oxides anions, 0.031(2) Å^2. Our joint refinement does not show any preferential occupation of the Mg cations in a given Ca site. However, due to the complexity of the structure we cannot completely rule out this possibility.

Our description of the disorder in the superstructure is simpler than that previously reported [24]. Nishi et al. structure contains 226 crystallographically independent sites and 540 refined positional parameters. However, the structure reported here fits better the well sample-averaged SXRPD and NPD patterns for alite. The structure for MIII reported by Mumme [23] is very much simpler with 21 sites and 48 refined positional parameters, but it does not fit alite properly. The *R* factors using exactly the same overall parameters and refining the scale factors, background parameters and unit cell ($a=12.200$ Å, $b=7.069$ Å, $c=9.275$ Å, $\beta=116.22°$) were: $R_{WP}=23.3\%$, $R_P=26.4\%$ and $R_F(C_3S)=17.2\%$ for the SXRPD data and $R_{WP}=15.5\%$, $R_P=11.5\%$ and $R_F(C_3S)=18.7\%$ for the NPD data. These values for the *R* factors are unacceptably high, and it rules out the use of the substructure for describing alite when analysing mixture of phases by Rietveld refinements.

Foreign ions (i.e. Mg^{2+}) induce the orientation of the SiO_4 tetrahedra, playing an important role to explain the

Table 2
Phase composition for the refinements of the Portland clinkers using our superstructure for alite (upper row) and the Nishi et al. [24] structure (italics)

Sample	C_3S/%	C_2S/%	C_4AF/%	C_3A/%	NKS[a]/%	C/%	C_3S+C_2S/%	CaO/%	SiO_2/%	Al_2O_3/%	Fe_2O_3/%	SO_3[b]/%	K_2O[c]/%	Na_2O[c]/%	MgO/%	CaO[d]/%
A1	67.4(2)	10.2(5)	12.8(3)	7.4(2)	2.2(2)	–	77.6	67.05	21.30	5.58	4.37	1.06	0.94	0.27	–	–
	67.9(2)	*10.0(5)*	*12.5(3)*	*7.4(2)*	*2.2(2)*	–	*77.9*									
	58.8	16.0	9.6	8.6	–	–	74.8	65.42	20.99	5.26	3.17	1.15	1.10	0.41	1.24	1.99
A2	48.9(2)	27.1(2)	15.5(2)	6.33(8)	1.83(6)	0.41(2)	76.0	65.46	22.32	6.81	3.65	0.88	0.78	0.27	–	0.41
	48.6(2)	*27.3(2)*	*15.6(5)*	*6.18(7)*	*1.93(6)*	*0.42(2)*	*75.9*									
	49.0	24.1	10.5	9.3	–	–	73.1	64.14	21.20	5.70	3.45	1.72	1.26	0.18	1.38	1.9
A3	64.2(3)	11.6(6)	16.3(3)	4.9(2)	3.0(2)	–	75.8	65.72	20.94	5.40	5.56	1.45	1.28	0.27	–	–
	65.4(3)	*11.3(5)*	*15.8(3)*	*4.5(2)*	*3.0(2)*	–	*76.7*									
	65.7	10.5	10.9	6.6	–	–	76.2	65.16	20.90	4.76	3.57	1.53	0.83	0.16	1.60	0.88
A4	62.5(3)	17.0(5)	13.3(3)	5.7(2)	1.4(1)	–	79.5	67.05	22.38	5.05	4.54	0.67	0.60	0.27	–	–
	62.6(3)	*17.0(5)*	*13.5(3)*	*5.7(2)*	*1.2(2)*	–	*79.6*									
	58.4	16.5	9.6	9.0	–	–	74.9	64.93	21.07	5.40	3.15	1.43	0.72	0.20	2.47	1.22

The third row is the mineralogical composition calculated by the Bogue method [41]. Elemental compositions derived from Rietveld results (upper row) and measured by XRF (third row) are expressed as parent oxide content.

[a] NKS stands for aphthitalite $NaK_3(SO_4)_2$.

[b] SO_3 was determined from gravimetry.

[c] Na and K were determined from emission spectroscopy.

[d] Free lime was determined from titrimetry.

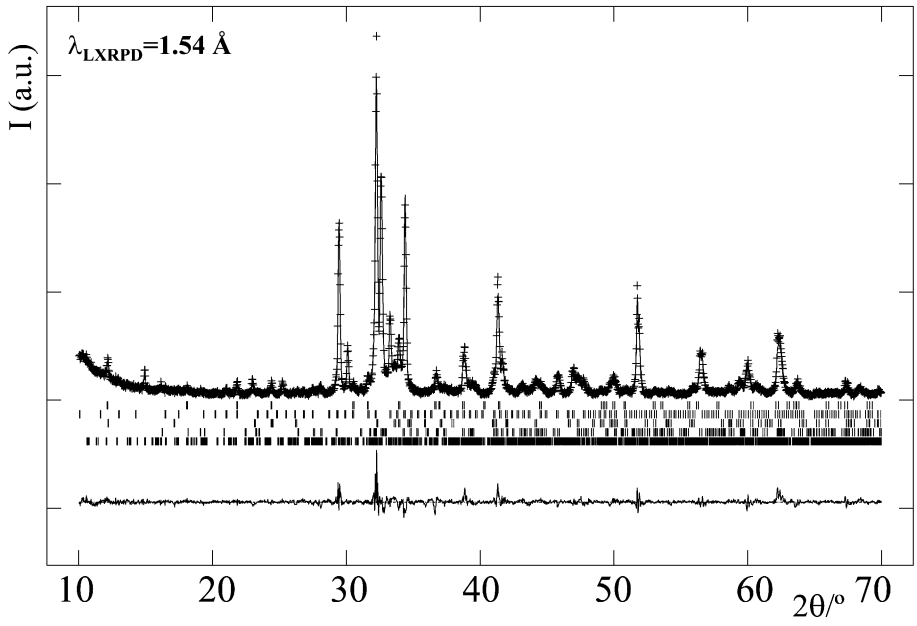

Fig. 3. LXRPD Rietveld plot for the A1 clinker.

disorder and the superstructure itself in MIII C_3S. In this context, it is worth pointing out that the single crystals of MIII C_3S investigated by Mumme [23] almost did not show the superstructure spots and their average MgO content was low, 0.76 wt.%. Our alite contains 1.24 wt.% of MgO, and the single crystal investigated by Nishi et al. [24] contained 1.96 wt.% of MgO. The unit cell volumes of these three MIII alites are 4328, 4303, and 4289 $Å^3$, respectively. Obviously, the unit cell volume decreases with the increasing of the Mg content.

3.2. Quantitative analyses of clinkers and cements

The results of the Rietveld analyses for four selected Portland clinkers with different Mg contents are given in Table 2. In Fig. 3, as an example, the Rietveld plot for the A1 clinker is shown. The references for the appropriated structures of the different phases are given at the bottom of Table 3. We do not have applied the microabsorption correction [37] since we have not characterised the particle sizes of the different phases. However, the absorption coefficients are given in Table 3. The amount of MgO in the clinkers is an important parameter in order to describe its powder pattern since it may induce slight changes in the superstructure of MIII alite. The wt.% of MgO in clinkers A1, A2, A3 and A4 are 1.24, 1.38, 1.60 and 2.47, respectively. Alite crystallises as large microcrystals, which show strong preferred orientation for front-loaded samples in the Bragg–Brentano reflection geometry. For this phase, we have tested both March–Dollase [38] and spherical–harmonic [39] corrections. The improvement with this last correction is larger in agreement with very recent results in Rietveld quantitative phase analysis [40].

From the results shown in Table 2, several conclusions can be drawn. (1) Both superstructures (Ref. [24] and ours) allow to describe alite satisfactorily. The fits, for complex disordered solid solutions, are acceptable with relatively smooth difference curves. The quality of the fits does not strongly depend on the Mg content, which encourages us since we do not need several structural descriptions for alite depending upon the Mg contents. (2) Due to the strong peak overlapping of C_3S and C_2S, we also give in Table 2 the

Table 3
Phase composition for the refinements of the Portland cements using our superstructure description for alite

Sample	C_3S/%	C_2S/%	C_4AF/%	C_3A/%	NKS/%	$CaSO_4 \cdot 2H_2O$/%	$CaSO_4 \cdot 1/2H_2O$/%	$CaCO_3$/%	MgO/%
B1	57.3(4)	14.9(5)	14.0(3)	5.4(2)	1.5(1)	0.85(8)	3.7(2)	2.4(2)	–
B2	58.0(4)	13.1(5)	13.9(4)	4.2(2)	1.3(2)	–	4.2(2)	4.5(2)	0.9(1)
B3	55.4(4)	15.2(5)	11.4(3)	6.3(2)	1.4(2)	0.63(8)	4.0(2)	4.8(2)	0.8(1)
B4	55.0(4)	15.9(5)	12.7(3)	5.0(2)	1.6(2)	–	4.5(2)	3.1(2)	2.1(1)
μ/cm $^{-1}$ [a]	305.5	295.1	425.0	261.0	200.9	136.3	191.1	192.0	99.7
[b]	Our work	[23]	[42]	[43]	[44]	[45]	[46]	[47]	[48]

[a] The absorption coefficients of the different phases for the CuKα radiation are given in this row.
[b] The references that contain the appropriated crystal structure descriptions are given in this row.

overall C_3S and C_2S contents for the clinkers. Bogue calculation invariably slightly underestimates this quantity. (3) The Bogue approach severely underestimates the C_4AF content and overestimates the C_3A.

Table 2 also shows the elemental compositions, expressed as parent oxide content, derived from Rietveld results and those measured by XRF. Although the overall agreement is quite good some remarks must be done. (1) Free lime content determined from LXRPD is always smaller than that from titrimetry as this last method also includes the amorphous fraction. Furthermore, the titrimetries were immediately carried out in the factory, but the Rietveld-quality LXRPD data were taken several days later at the University. So, partial carbonation can be expected. (2) CaO is always overestimated in the Rietveld results as it includes the Ca/Mg substitution which cannot be modeled. Consequently, MgO is severely underestimated. However, the results are consistent and the CaO + MgO elemental composition determined by XRF agrees very well (inside 1%) with the CaO elemental composition determined by the Rietveld study. (3) Similarly, SiO_2 is always slightly overestimated in the Rietveld analysis as the Si/Al substitution cannot be taken into account. (4) The agreement for Fe_2O_3 is not very satisfactory probably due to the nominal stoichiometry (1:1) used to model C_4AF. However, there is not enough information in the LXRPD data for the refinement of the Fe/Al occupation factors in C_4AF. (5) Finally, the SO_3 content is slightly underestimated in the Rietveld analyses. This is not surprising as sulfates are the last fraction to crystallize, and it can remain partially amorphous.

The results of the Rietveld analyses for four selected Portland cements are given in Table 3. In Fig. 4, as an example, the Rietveld plot for the B1 cement is shown. The samples contained up to nine crystalline phases, but the refinements were stable and the fits were satisfactory as indicated by the smoothness of the difference curve in Fig. 4. The wt.% of MgO in cements B1, B2, B3 and B4 are 1.53, 1.68, 2.10 and 2.53, respectively.

Preferred orientation had to be also applied to some phases in cements with $CaSO_4{\cdot}2H_2O$ and $CaSO_4{\cdot}1/2H_2O$ being the extreme cases. March–Dollase correction [38] gave good fits, and it has a unique refinable parameter per phase, so this correction was used for all phases excepting alite. The results are consistent, when $CaSO_4{\cdot}2H_2O$ was detected, then a lower content of $CaSO_4{\cdot}1/2H_2O$ was measured. Therefore, quantitative mineralogical analyses of Portland cements allow even the analysis of dehydration reactions of gypsum in the cement ball mills. The content range of all phases were found to lie within the expected values for the Portland cement.

4. Conclusions

We report a simpler structural description for the superstructure of MIII alite from a combined SXRPD, NPD and interatomic distances soft-constrained Rietveld refinement. This structure has been proven to refine properly a variety of Portland clinker and cement specimens. The Rietveld quantitative analyses of four clinkers with variable Mg contents have shown that the refinements are of good quality and that the Bogue approach repeatedly underestimates the $C_3S + C_2S$ content, overestimates the C_3A fraction and underestimates the C_4AF content. Similar analyses of Portland cements with nine crystalline phases are feasible and even

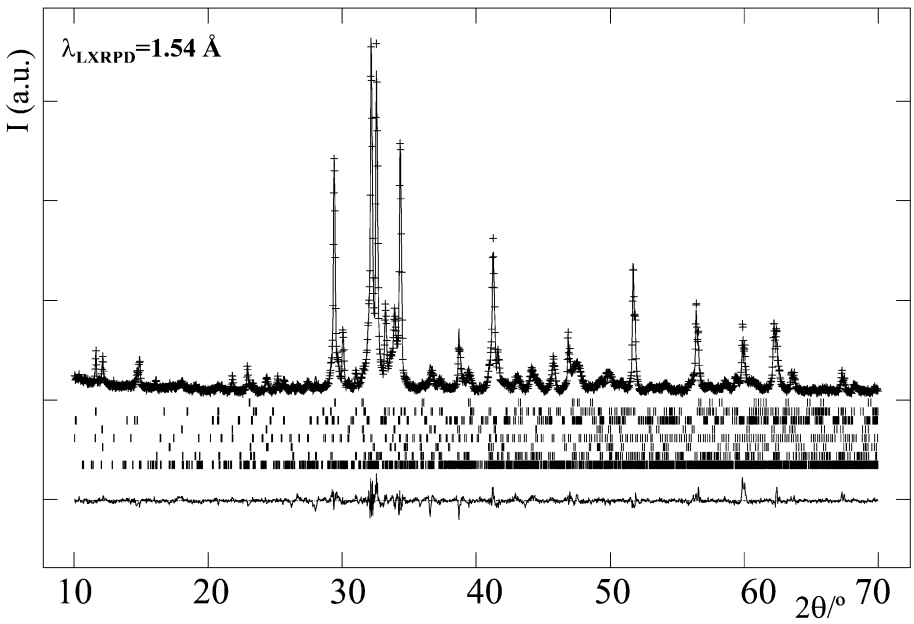

Fig. 4. LXRPD Rietveld plot for the B1 cement.

allows data regarding dehydration reactions in the cement ball mills.

Acknowledgments

ESRF and ILL are thanked for the provision of X-ray synchrotron and NPD facilities, respectively. This work has been supported by the FEDER 1FD97-0894 research grant.

References

[1] C. Manias, D. Retallack, I. Madsen, XRD for on-line analysis and control, World Cem. (2000) 78–81 (February).
[2] N.V.Y. Scarlett, I.C. Madsen, On-line X-ray diffraction for quantitative phase analysis: Application in the Portland cement industry, Powder Diffr. 16 (2) (2001) 71–80.
[3] A.G. De La Torre, A. Cabeza, A. Calvente, S. Bruque, M.A.G. Aranda, Full phase analysis of Portland clinker by penetrating synchrotron powder diffraction, Anal. Chem. 73 (2001) 151–156.
[4] J.C. Taylor, I. Hinczak, C.E. Matulis, Rietveld full-profile quantification of Portland cement clinker: The importance of including a full crystallography of the major phase polymorphs, Powder Diffr. 15 (1) (2000) 7–18.
[5] R. Schmidt, A. Kern, Quantitative XRD phase analysis, World Cem. (2001) 2–8 (February).
[6] A. Kern, Accurate quantitative XRD phase analysis of cement clinkers, Accuracy in Powder Diffraction III, NIST, Gaithersburg, USA, 2001.
[7] P.E. Stutzman, S. Leigh, Compositional analysis of NIST reference material clinker 8486, Accuracy in Powder Diffraction III, NIST, Gaithersburg, USA, 2001.
[8] J. Neubauer, R. Sieber, Quantification of synthetic alite and belite by the Rietveld method, Mater. Sci. Forum 228–231 (1996) 807–812.
[9] J. Neubauer, Introduction of Rietveld quantitative phase analysis in OPC clinker production, Proceedings of the 20th International Conference On Cement Microscopy, Guadalajara, Mexico, International Cement Microscopy Association, Duncanville, Texas, 1998, pp. 103–119.
[10] F. Guirado, S. Galí, S. Chinchón, Quantitative Rietveld analysis of aluminous cement clinker phases, Cem. Concr. Res. 30 (2000) 1023–1029.
[11] R. Schmidt, H. Pöllmann, Quantification of calcium sulpho-aluminate cement by Rietveld analysis, Mater. Sci. Forum 321–324 (2000) 1022–1027.
[12] L.P. Aldridge, Accuracy and precision of phase analysis in Portland cement by Bogue, microscopic and X-ray diffraction methods, Cem. Concr. Res. 12 (1982) 381–398.
[13] L.P. Aldridge, Accuracy and precision of an X-ray diffraction method for analysing Portland cements, Cem. Concr. Res. 12 (1982) 437–446.
[14] F.P. Glasser, Methods for the determination of clinker phase composition, in: P.C. Hewlett (Ed.), Lea's Chemistry of Cement and Concrete, Arnold, London, 1998, pp. 196–227.
[15] W.A. Gutteridge, Quantitative X-ray powder diffraction in the study of some cementive materials, in: F.P. Glasser (Ed.), British Ceramics Proceedings No. 35: The Chemistry and Chemical Related Properties of Cement, British Ceramic Society, Stoke on Trent, UK, 1984, p. 11–23.
[16] H.M. Rietveld, A profile refinement method for nuclear and magnetics structures, J. Appl. Crystallogr. 2 (1969) 65–71.
[17] R.A. Young, The Rietveld Method, Oxford Univ. Press, Oxford, 1993.
[18] L.B. McCusker, R.B. Von Dreele, D.E. Cox, D. Louer, P. Scardi, Rietveld refinements guidelines, J. Appl. Crystallogr. 32 (1999) 36–50.
[19] N.I. Golovastikov, R.G. Matveeva, N.V. Belov, Crustal structure of the tricalcium silicate $3CaO{\cdot}SiO_2{=}C_3S$, Sov. Phys. Crystallogr. 20 (4) (1975) 441–445.
[20] K. Urabe, T. Shirakami, M. Iwashima, Superstructure in a triclinic phase of tricalcium silicate, J. Am. Ceram Soc. 83 (5) (2000) 1253–1258.
[21] H.F.W. Taylor, Cement Chemistry, Thomas Telford, London, 1997.
[22] I. Maki, K. Kato, Phase identification of alite in Portland cement clinker, Cem. Concr. Res. 12 (1982) 93–100.
[23] W.G. Mumme, Crystal structure of tricalcium silicate from a Portland cement clinker and its application to quantitative XRD analysis, Neues Jahrb. Mineral. 4 (1995) 145–160.
[24] F. Nishi, Y. Takeuchi, I. Maki, Tricalcium silicate $Ca_3O[SiO_4]$: the monoclinic superstructure, Z. Kristallogr. 172 (1985) 297–314.
[25] F. Nishi, Y. Takeuchi, The rhombohedral structure of tricalcium silicate at 1200 °C, Z. Kristallogr. 168 (1984) 197–212.
[26] M. Belloto, M. Signes-Frehel, Contribution à la détermination de la structure de l'alite par diffraction des rayons X sur poudres, J. Phys. IV 8 (1998) 511–518.
[27] A. Cabeza, E.R. Losilla, H.S. Martínez-Tapia, S. Bruque, M.A.G. Aranda, Disorder polycrystalline materials: Applications to Rietveld refinements, Adv. X-ray Anal. 42 (2000) 228–237.
[28] J. Hjorth, J. Skibsted, H.J. Jakobsen, ^{29}Si MAS NMR studies of Portland cement components and effects of microsilica on the hydration reaction, Cem. Concr. Res. 18 (1988) 789–798.
[29] R. Berliner, C. Ball, P.B. West, Neutron powder diffraction investigation of model cement compounds, Cem. Concr. Res. 27 (4) (1997) 551–575.
[30] D.E. Simon, Discussion of the paper "Neutron powder diffraction investigation of model cement compounds", Cem. Concr. Res. 28 (12) (1998) 1833–1836.
[31] R. Berliner, C. Ball, P.B. West, Reply to the discussion of the paper "Neutron powder diffraction investigation of model cement compounds" by Berliner et al., Cem. Concr. Res. 28 (12) (1998) 1831–1832.
[32] A.C. Larson, R.B.Von Dreele, General Structural Analysis System, Los Alamos National Lab. Rep. No. LA-UR-86-748, 1994.
[33] P. Thompson, D.E. Cox, J.B. Hasting, Rietveld refinement of Debye–Scherrer synchrotron X-ray data from Al_2O_3, J. Appl. Crystallogr. 20 (1987) 79–83.
[34] L.W. Finger, D.E. Cox, A.P. Jephcoat, A correction for powder diffraction peak asymmetry due to diaxial divergence, J. Appl. Crystallogr. 27 (1994) 892–900.
[35] M.A.G. Aranda, E.R. Losilla, A. Cabeza, S. Bruque, Effective correction of peak asymmetry: Rietveld refinement of high-resolution synchrotron powder data of $Li_{1.8}(Hf_{1.2}Fe_{0.8})(PO_4)_3$, J. Appl. Crystallogr. 31 (1998) 16–21.
[36] W.G. Mumme, R.J. Hill, G. Bushnell-Wye, E.R. Segnit, Rietveld structure refinement, crystal chemistry and calculated powder diffraction data for the polymorphs of dicalcium silicate and related phases, Neues Jahrb. Miner. Abh. 169 (1995) 35–68.
[37] G.W. Brindley, The effect of grain or particle size on X-ray reflection from mixed powders and alloys, considered in relation to the quantitative determination of crystalline substances by X-ray methods, Philos. Mag. 36 (1945) 347–369.
[38] W.A. Dollase, Correction of intensities for preferred orientation in powder diffractometry: Application of the March model, J. Appl. Crsytallogr. 19 (1986) 267–272.
[39] R.B. Von Dreele, Quantitative texture analysis by Rietveld refinement, J. Appl. Crystallogr. 30 (1997) 517–525.
[40] I.C. Madsen, N.V.Y. Scarlett, L.M.D. Cranswick, T. Lwin, Outcomes of the International Union of Crystallography Commission on powder diffraction round robin on quantitative phase analysis: Samples 1a to 1 h, J. Appl. Crystallogr. 34 (2001) 409–426.
[41] R.H. Bogue, Ind. Eng. Chem. (Anal. Ed.) 1 (1929) 192.
[42] A.A. Coville, S. Geller, The crystal structure of Brownmillerite, Ca_2FeAlO_5, Acta Crystallogr. B 27 (1971) 2311–2315.
[43] P. Mondal, J.W. Jeffery, The crystal structure of tricalcium aluminate, $Ca_3Al_2O_6$, Acta Crystallogr. B 31 (1975) 689–697.

[44] K. Okada, J. Ossaka, Structures of potassium sodium sulphate and tripotassium sodium disulphate, Acta Crystallogr. B 36 (1980) 919–921.
[45] P.F. Schofield, K.S. Knight, I.C. Stretton, Thermal expansion of gypsum investigation by neutron powder diffraction, Am. Mineral. 81 (1996) 847–851.
[46] C. Bezou, A. Nonat, J.C. Mutin, A.N. Christensen, M.S. Lehmann, Investigation of the crystal structure of gamma-$CaSO_4$, $CaSO_4 \cdot 0.5H_2O$ and $CaSO_4 \cdot 0.6H_2O$ by powder diffraction methods, J. Solid State Chem. 117 (1995) 165–176.
[47] E.N. Maslen, V.A. Streltsov, N.R. Streltsova, N. Ishizawa, Electron density and optical anisotropy in rhombohedral carbonates: III. Synchrotron X-ray studies of $CaCO_3$, $MgCO_3$ and $MnCO_3$, Acta Crystallogr. B 51 (1995) 929–939.
[48] S. Sasaki, K. Fujino, Y. Takeuchi, X-ray determination of electron-density distributions in oxides, MgO, MnO, CoO, and NiO, and atomic scattering factors of their constituent atoms, Proc. Jpn. Acad. 55 (1979) 43–48.